Journal of Materials Science: Materials in Medicine (2019) 30:98
https://doi.org/10.1007/s10856-019-6297-8

BIOMATERIALS SYNTHESIS AND CHARACTERIZATION

Original Research

Effect of ethanol/TEOS ratios and amount of ammonia on the properties of copper-doped calcium silicate nanoceramics

Georgia K. Pouroutzidou[1] · Georgios S. Theodorou[1] · Eleana Kontonasaki[2] · Ioannis Tsamesidis[3] · Antonella Pantaleo[3] · Dimitra Patsiaoura[1] · Lambrini Papadopoulou[4] · Jonathan Rhoades[5] · Eleni Likotrafiti[5] · Christos B. Lioutas[1] · Konstantinos Chrissafis[1] · Konstantinos M. Paraskevopoulos[1]

Received: 6 June 2019 / Accepted: 31 July 2019 / Published online: 22 August 2019

Abstract

Calcium magnesium silicate glasses could be suggested for the synthesis of scaffolds for hard tissue regeneration, as they present a high residual glassy phase, high hardness values and hydroxyapatite-forming ability. The use of trace elements in the human body, such as Cu, could improve the biological performance of such glasses, as Cu is known to play a significant role in angiogenesis. Nano-bioceramics are preferable compared to their micro-scale counterparts, because of their increased surface area, which improves both mechanical properties and apatite-forming ability due to the increased nucleation sites provided, their high diffusion rates, reduced sintering time or temperature, and high mechanical properties. The aim of the present work was the evaluation of the effect of different ratios of Ethanol/TEOS and total amount of the inserted ammonia to the particle size, morphology and bioactive, hemolytic and antibacterial behavior of nanoparticles in the quaternary system SiO_2–CaO–MgO–CuO. Different ratios of Ethanol/TEOS and ammonia amount affected the size and morphology of bioactive nanopowders. The optimum materials were synthesized with the highest ethanol/TEOS ratio and ammonia amount as verified by the enhanced apatite-forming ability and antibacterial and non-hemolytic properties.

Graphical Abstract

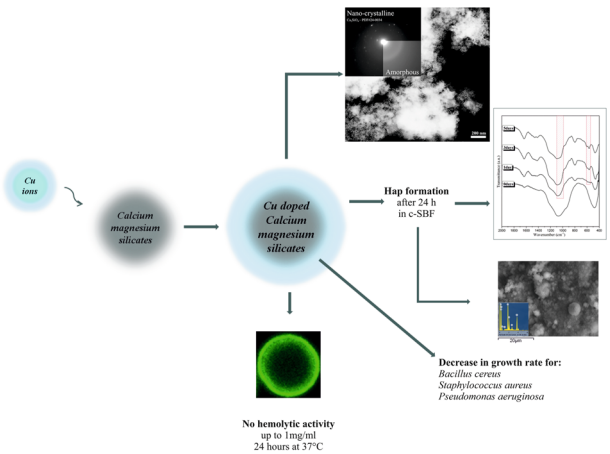

✉ Eleana Kontonasaki
kont@dent.auth.gr

[1] School of Physics, Faculty of Sciences, Aristotle University of Thessaloniki, 54124 Thessaloníki, Greece

[2] Department of Fixed Prosthesis and Implant Prosthodontics, School of Health Sciences, Faculty of Dentistry, Aristotle University of Thessaloniki, 54124 Thessaloniki, Greece

[3] Department of Biomedical Sciences, University of Sassari, Sassari 07100, Italy

[4] Department of Mineralogy-Petrology-Economic Geology, School of Geology, Faculty of Sciences, Aristotle University of Thessaloniki, 54124 Thessaloniki, Greece

[5] Department of Food Technology, Alexander Technological Educational Institute of Thessaloniki, Thessaloniki 57 400, Greece

1 Introduction

Nanotechnology is rapidly sweeping through all vital fields of science and technology, including medicine and dentistry, and involves the design, synthesis, characterization, and application of materials and devices of particles with at least one dimension in the nanometer scale (10–100 nm in diameter) [1–3]. It has drawn a great interest of research owing to its potential to improve biomaterials used in tissue engineering [2]. Tissue function could be improved with the use of engineering systems for controlled release of biological nanomolecules and supplementing scaffolds with inorganic nanoparticles [4].

Due to the strong need for the replacement of large segments of diseased and defective hard tissue, such as bone, cartilage, and teeth, nanoscale bioceramics containing ions with proved efficacy in promoting cell proliferation and differentiation towards osteogenic or odontogenic lineage cells, could remarkably enhance the performance of many dental and biomedical materials [3, 5]. In order to create devices or systems with reconstruction properties, nanobioceramics are more preferable in tissue engineering compared to their micro-scale counterparts, because of their increased surface area, which improves both mechanical properties and apatite forming ability due to the increased nucleation sites provided [3, 6].

The sol-gel method is a wet-chemistry process for producing materials such as silica nanoparticles controlling the particle size and shape, size distribution, and morphology [7–22].

Due to the sensitivity of the experimental conditions during the sol-gel synthesis, the rate of hydrolysis and condensation reactions of the solution could be affected by the type and concentration of starting materials (alkoxides), catalyst's nature and concentration/pH, nature of solvent, temperature, aging and drying method [23–28]. According to the Stöber's method, the use of ammonia as catalyst of hydrolysis and condensation of ethoxysilanes in the presence of low molecular-weight alcohols as solvent, such as ethanol, could successfully lead to the production of uniform silica based nanoparticles [17, 23, 29–39]. However, many factors could affect the size of nanoparticles and their distribution, such as the concentration of TEOS, H_2O, and NH_3, the amount and nature of the alkohol (solvent), as well as the reaction temperature [17, 29].

Recently, calcium silicate based ceramics have attracted great attention as potential bioactive bone graft materials since they have shown high ability to induce in vitro osteogenesis and in vivo bone regeneration, excellent bioactivity and biodegradable properties, via the release of calcium and silicon ions into the surrounding environment [40–44]. Recent studies demonstrated that the incorporation of an additional inorganic component with specific biological activity, such as strontium (Sr), zinc (Zn), or magnesium (Mg) could improve the physicochemical and biological properties of calcium silicate glass–ceramics [45–51]. Specifically, Mg-containing silicate glasses exhibit prolonged degradation rates, a high residual glassy phase, optimum hardness values and hydroxyapatite-forming ability so, they could be suggested for the synthesis of scaffolds for hard tissue regeneration [52, 53].

Although bioactive glasses have been widely used in bone tissue engineering due to their osteoinductive behavior, angiogenesis still remains a problem. Lately, many studies have been conducted to improve the angiogenic properties of bioceramics, due to the need of tissue vascularization for hard tissue regeneration applications [54]. The use of trace elements in the human body, such as copper (Cu), could improve the performance of such glasses, as Cu is known to play a significant role in angiogenesis, blood vessel maturation, provides beneficial effects to induce differentiation of MSCs and improves the antibacterial potential [55, 56].

Lately, calcium silicate bioactive glasses have been used as a potential alternative to the systemic delivery of antibiotics for prevention against bacterial infections as they provide intrinsic antibacterial properties [57]. Despite various bioceramic systems, their hemolytic properties, that determine the red blood cell dissolution and the hemoglobin dissociation rates, it has not been thoroughly investigated, although erythrocytes and blood are the primary cells and fluid respectively, that will come in contact with bone implantation materials [58].

The aim of the current study was the synthesis of nanoparticles in the quaternary system SiO_2–CaO–MgO–CuO and the evaluation of the effect of different ratios of Ethanol/TEOS as well as the total amount of the inserted ammonia to their particle size, morphology and bioactive behavior. The antibacterial and hemolytic properties of the optimum material in terms of bioactivity were further investigated.

2 Materials and methods

2.1 Synthesis of bioactive glasses

Sol–gel derived bioactive glass nanopowders (BGs) were prepared according to a previously reported method with some modification, with composition in mol%: 60 SiO_2, 30 CaO, 7.5 MgO and 2.5 CuO [59]. BGs were produced by the hydrolysis of TEOS in a mixture of d.d. H_2O, ethanol and $HNOf_3$. Ca, Mg and Cu were added as nitrate salts while ammonia solution was inserted dropwise under stirring and sonication (Table 1). After the gelation of the solutions, the prepared gels were dried at 75 °C for 48 h and

Table 1 Ratios of Ethanol/TEOS, H_2O/TEOS, Ethanol/H_2O and H_2O/Ethanol and amount of ammonia of compositions

a/a	Ethanol/TEOS	Ammonia (ml)	H_2O/TEOS	Ethanol/H_2O	H_2O/Ethanol
BG 1	1	20	12	0.083	12
BG 2	5	20	12	0.42	2.4
BG 3	10	20	12	0.83	1.2
BG 4	1	5	12	0.083	12
BG 5	5	5	12	0.42	2.4
BG 6	10	5	12	0.83	1.2

then subjected to heat treatment at 700 °C for 3 h with a heating rate of 3 °C/min to stabilize and convert gels to glasses.

2.2 Characterization

2.2.1 Thermogravimetric analysis and differential thermal analysis (TG-DTA)

The thermal decomposition of the dried gels were studied in nitrogen atmosphere by using thermogravimetric analysis and differential thermal analysis (TG-DTA) performed from room temperature to 1300 °C, with a heating rate of 10 °C min^{-1}.

2.2.2 Fourier transform infrared spectroscopy (FTIR)

In order to determine the chemical composition of the nanopowders, all samples were characterized by Fourier Transform Infrared Spectroscopy (Perkin-Elmer Spectrometer Spectrum 1000) and the spectra were collected in the transmittance mode in the range of 400–4000 cm^{-1}. Pellets of all nanopowders with powder to KBr ratio of 1:100 were fabricated under pressure (7 tons).

2.2.3 X-ray diffraction (XRD)

For the XRD analysis, a Rigaku Ultima diffractometer with Ni-filtered CuKa radiation ($\lambda = 0.1542$ Å) wave radiation was used. The XRD patterns were recorded in the 2θ range of 5°–75°, with a step size of 0.02° and scanning speed of 0.008° 2θ/s.

2.2.4 Scanning electron microscopy and energy dispersive spectroscopic analysis (SEM-EDS)

The microstructure and morphology of all samples was determined by the use of Scanning Electron Microscopy with associated Energy Dispersive Spectroscopic Analysis (SEM-EDS) was used (SEM) JEOL JSM-6390LV and JEOL JSM- 84OA spectrometers.

2.2.5 Transmission electron microscopy (TEM)

TEM (JEOL 1010) operating at 100 KV was used to analyze the morphology and particle size of all synthesized nanomaterials.

2.3 Apatite forming ability in SBF

Nanopowders were placed in sterilized reagent bottles and submerged in SBF solution with mass to solution ratio adjusted at 1.5 mg/mL [60]. Then they were placed in an incubator (Incucell 55) at 37 °C under renewal conditions for various times after immersion (6, 24 h, and then after every 48 h) [61]. Finally the specimens were centrifuged and precipitates were removed from the SBF at each time point (after 1, 3 and 5 days of immersion) and dried at room temperature.

2.4 Hemolytic activity

Fresh human heparinized whole blood was obtained from healthy volunteer donors. Volunteers provided written, informed consent before entering the study. The study was conducted in accordance with Good Clinical Practiceguidelines and the Declaration of Helsinki. Ethical approval to perform thepresent study was obtained from the Ethical committee of the ASL.1-Sassari. Red Blood Cells (RBCs) were separated from plasma and leukocytes by washing three times with phosphate buffered saline (PBS). To determine the haemolytic activity on RBCs, nanoparticles suspension (stock = 1 mg/ml) prepared with sterile isotonic PBS 1×, was added to diluted RBCs at different concentrations (0.25, 0.5, 1, 2.5, 5, 7.5 mg/ml) for 24 and 48 h of incubation at 37 and 41 °C (Thermomixer-Biosan). Testing both temperature conditions is of particular interest for bioactive glass nanomaterials, as they should be used for therapeutic/healing purposes, which might encounter complex conditions such as fever. PBS 1× was used as a negative control (Ctrl−) and hemolysis buffer (5 mmol/L sodium phosphate, 1 mmol/L EDTA, pH 8.0) was used as positive control (Ctrl+). Then, samples were centrifuged at 2000 rpm for 1 min and a microplate reader (Thermo Scientific) was used to measure the absorbance of haemoglobin release in the supernatant. The absorbance value of haemoglobin at 541 nm was measured with the reference wavelength of 700 nm. The percent of hemolysis was calculated as follows: Hemolysis % = [(sample absorbance − negative control)/(positive control − negative control)] * 100%. Significant differences between means were determined by two tailed t-test. Results of statistical analysis are expressed as mean ± SEM unless otherwise noted.

2.5 Bacterial cultures

Bacterial cultures were prepared as follows for each of the seven bacterial strains. Nutrient broth (NB, 10 mL) was inoculated from a stored culture on nutrient agar and incubated overnight at 37 °C. A 0.1 ml aliquot of the fresh broth culture was then inoculated into 10 ml NB and incubated for 24 h at 37 °C. Just before use, 1 ml of the 24 h culture was centrifuged (13,000 × g, 6 min) and the supernatant discarded. The precipitate was then resuspended in 1 ml NB, diluted 1:100 in NB and this suspension was used as the inoculum for the growth rate determination. The viable count of the remaining 24 h culture was determined by plating onto plate count agar and incubating for three days at 37 °C before colonies were enumerated.

Microtitre plates (Bioscreen) were prepared as follows. All wells were prepared in triplicate and all contained 300 µL total liquid. Test wells were prepared with 120 µL double-strength NB (dsNB), 150 µL substance BG3 (1 mg/mL aqueous suspension) and 30 µL of bacterial culture. Concentrations in the well were therefore 0.5 mg/mL substance BG3 and approximately 10^6 cfu/mL bacteria (1:1000 dilution of the 24 h culture). The dsNB was diluted to approximately normal strength by the aqueous suspension of substance BG3. In addition to the test wells, two types of controls were prepared. Normal growth of the bacteria was determined by placing 270 µL NB and 30 µL culture in the wells. The effect of substance BG3 on the optical properties of the suspension was determined by filling wells with 120 µL dsNB, 150 µL substance BG3 and 30 µL sterile NB.

Growth of the bacteria with and without substance BG3 was determined using the Bioscreen reader with the following settings: wavelength 580 nm, temperature 37 °C, measurement every 30 mins, experiment duration 24 h, shaking before measurement. The experiment was repeated twice to give three runs in total. At the end of the experiment, data was exported to Microsoft Excel for processing. For each triplicate measurement data was adjusted for initial absorbance by subtracting the mean of the time zero values from all measurements. Semi-log graphs were plotted of optical density (OD) against time, the period of maximum exponential growth was selected and the growth rate over the selected period calculated using the formula

$$\text{Growth rate} = \ln\left(\frac{\text{OD}t_2}{\text{OD}t_1}\right)/t_2 - 1, \quad (1)$$

where t_1 is the first time point of the selected exponential growth period and t_2 is the last. The growth rates of the substance-free controls and the test wells in each of the three runs were normalized by dividing each individual value by the mean of the three control values. Data from the three runs were then combined and the normalized growth rates in the test wells compared with those in the control wells ($n = 9$). Lag phases were approximated by determining the time before an increase in absorbance of at least 0.01 absorbance units was observed at the start of growth.

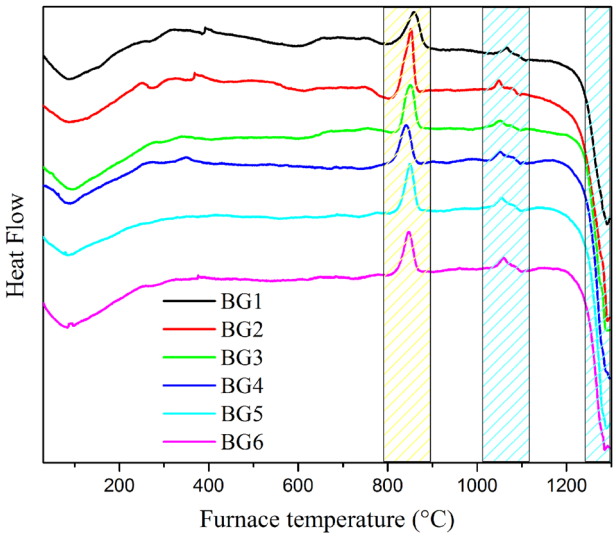

Fig. 1 DSC curves of all samples

3 Results

3.1 Thermogravimetric analysis and differential scanning calorimetry (TG-DSC)

The Heat-Flow curves of all samples (Fig. 1) exhibited two endothermic peaks up to 200 °C, which were attributed to the processes of water evaporation. Crystallization peaks were detected around 850 °C and two smaller crystallizations around 1050 and 1080 °C. The melting process starts approximately at 1150 °C.

Figure 2 shows the mass loss and the heat flow curves of all samples. Mass reduction in TG curves took place in four individual steps. Two first mass loss steps, which were overlapped, are attributed to water elimination, probably due to the evaporation of adsorbed water and resulting water during the polycondensation reaction of silanol [23, 29]. The most pronounced mass reduction occurred up to 200 °C resulting up to 3% mass loss, while the total mass loss at 1300 °C was well under 10%.

3.2 Fourier transform infrared spectroscopy (*FTIR*) measurements

The FTIR spectra of all nanopowders before soaking in SBF are presented in Fig. 3. The characteristic bands of silicate glasses are observed in all spectra, assigned to the broad

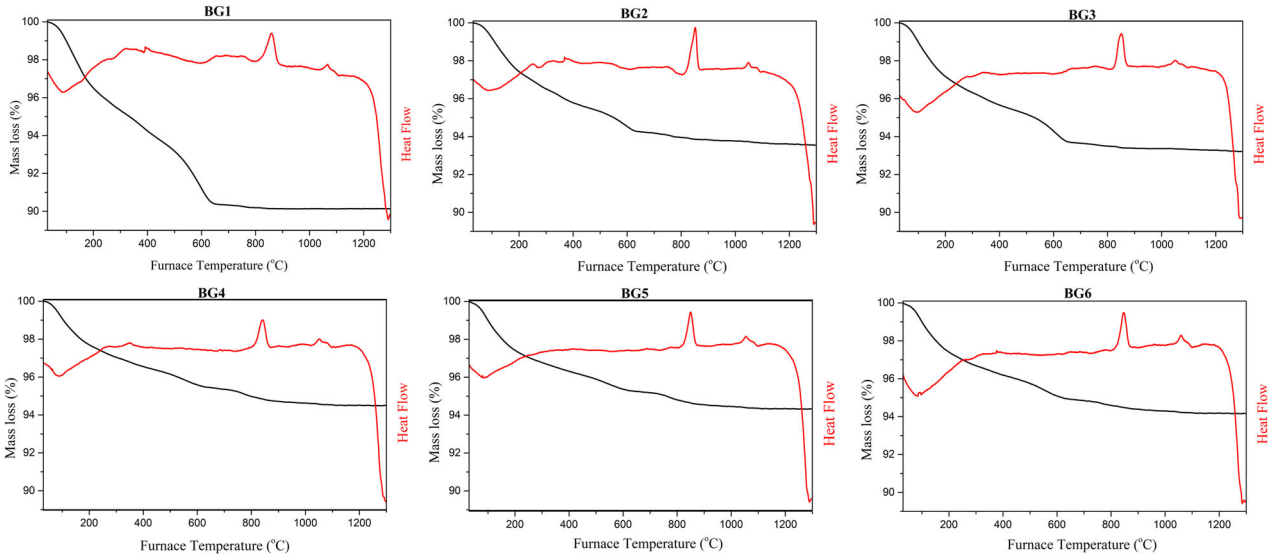

Fig. 2 Heat Flow and Mass Loss curves of all samples

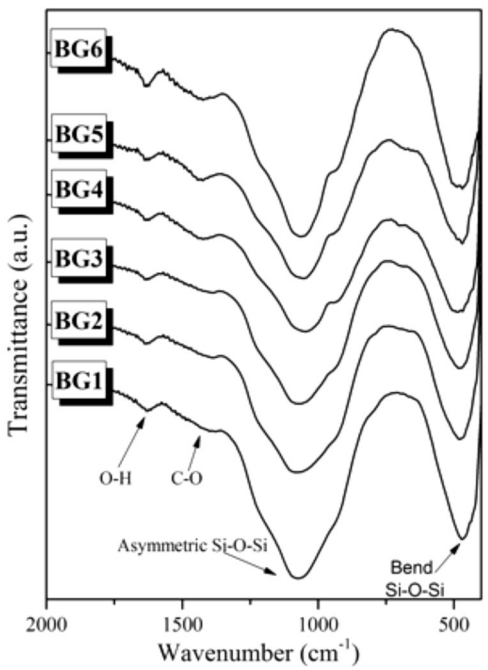

Fig. 3 FTIR spectra of produced biomaterials before soaking in SBF

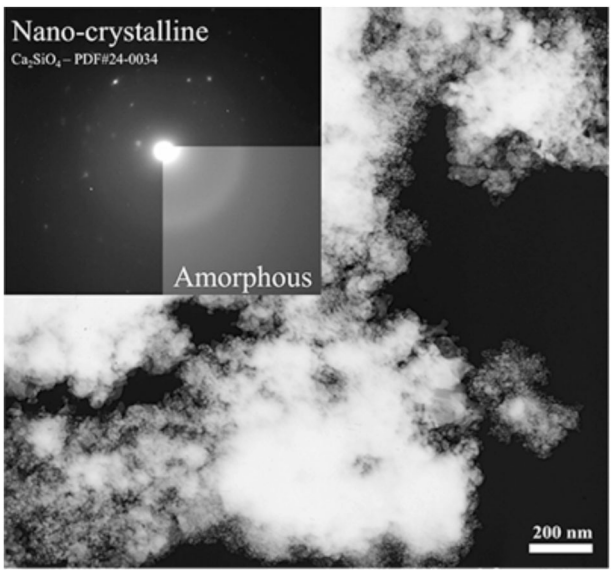

Fig. 4 TEM microphotograph and exemplary ED pattern of **BG3**

peak at 900–1200 cm^{-1} attributed to the asymmetric stretching vibration of Si–O–Si and the peak around 470 cm^{-1} attributed to the bending vibration of the Si–O–Si bonds [31, 62]. Moreover, the peak around 1645 cm^{-1} indicated the presence of absorbed water on the surface of the samples [32, 33] and the contribution of the C-O vibrations was observed in the range of 1410–1510 cm^{-1} due to stretching vibrations and in the range of 860–880 cm^{-1} due to out-of-plane bend [33].

3.3 Transmission electron microscopy (TEM)

TEM microphotographs of all samples show the coexistence of both nano-crystalline and amorphous phases. The size of the nano-agglomerates of all compositions was less than 100 nm, while *BG 3* (Fig. 4) consisted of agglomerates with the smallest size (6 nm). The electron diffraction (ED) pattern of the **BG3** indicates the formation of Ca_2SiO_4 (Fig. 4a). The size of the nano-agglomerates decreased as the amount of the inserted ammonia and the ratio of Ethanol/TEOS were increased. Simultaneously, the amorphous proportion of the glass-ceramic material was increased.

3.4 X-ray diffraction (XRD)

XRD patterns of the samples are shown in Fig. 5. The results are in accordance with the FTIR and ED patters of TEM findings. All bioactive glasses are consisted of a high amount of an amorphous phase (91–93%), while differences were observed among the crystalline phases of sample BG1 and BG2, BG4, BG5 and BG6. Specifically, a crystalline phase of Calcite ($CaCO_3$) was detected in sample BG1, BG2, and BG3. Moreover, an amount of Calcium Silicate (Ca_2SiO_4) was detected in samples BG3 (2–7%), BG4, BG5, and BG6 (5–9%). The total percentage of crystalline phases resulted up to 9%.

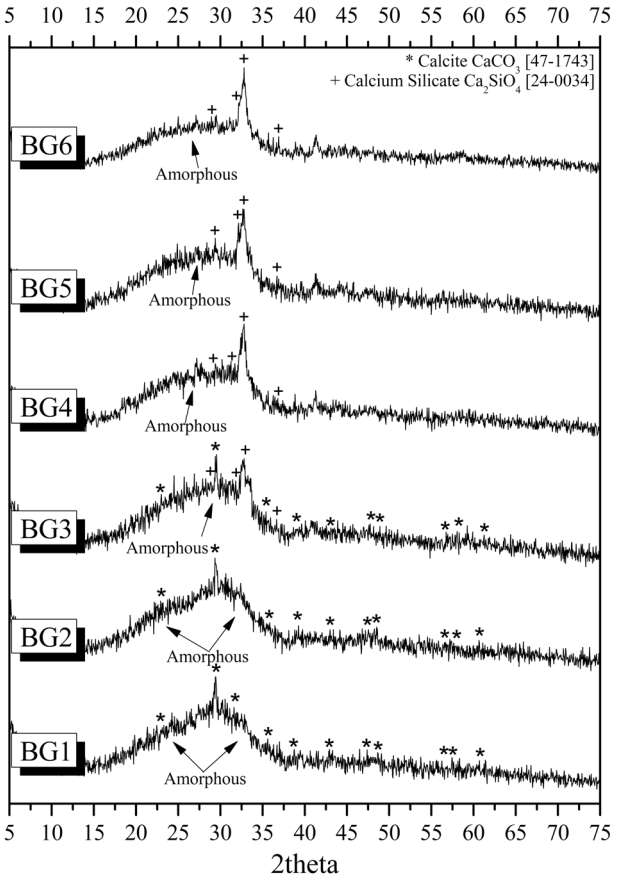

Fig. 5 XRD patterns of all bioactive glass before the immersion in SBF

3.5 Scanning electron microscopy and energy dispersive spectroscopic analysis (SEM-EDS)

The sample with increasing amount of ammonia before the immersion in SBF (0 days) consisted of aggregates exhibiting a large amount of small size dispersed grains, while the small amount of ammonia seems to lead to aggregates of augmented compactibility, showcasing diminished grain dispersion (Fig. 6).

3.6 Apatite forming ability in SBF

Figure 7 shows the FTIR spectra of the samples (BG1, BG2, BG3, BG4, BG5, and BG6) after soaking in SBF for 1, 3, and 5 days. After soaking for 24 h, the spectra of BG3 revealed the precipitation of apatite on the surface of the sample, as verified by the shifting and sharpening of the broad peak at 900–1200 cm^{-1} towards lower wavenumbers attributed to the bending of the $(PO_4)^{3-}$ group and the appearance of the two bands at 610 – 600 and 560 – 550 cm^{-1} assigned to the P–O bending vibration of Hap [63–65]. Furthermore, the presence of the peak at 780–800 cm^{-1} corresponds to the Si–O–Si stretching vibration due to the polycondensation of silanols [65]. It seems that apatite formation starts earlier on the sample BG3 compare to other samples, whose spectra revealed the formation of an

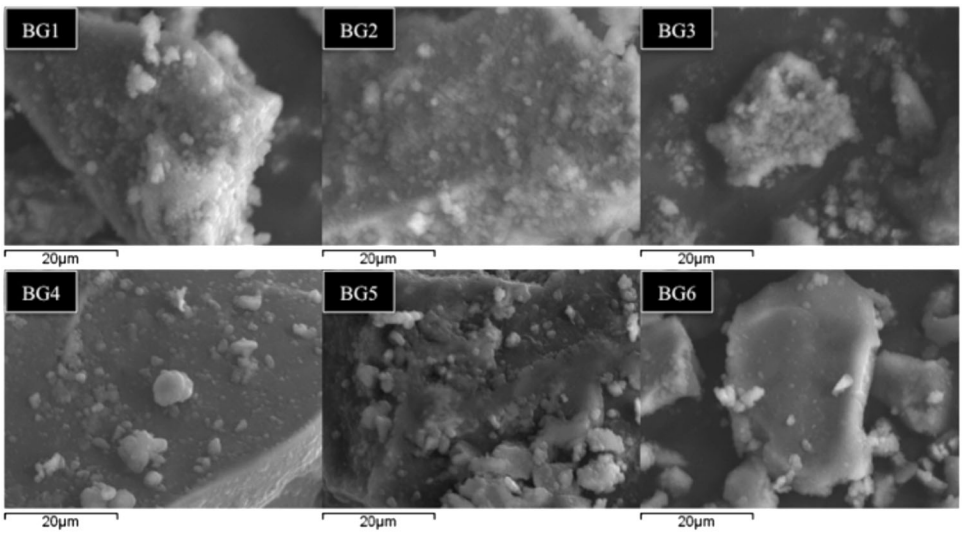

Fig. 6 SEM microphotographs of samples BG1, BG2, BG3, BG4, BG5 and BG6 before the immersion in SBF

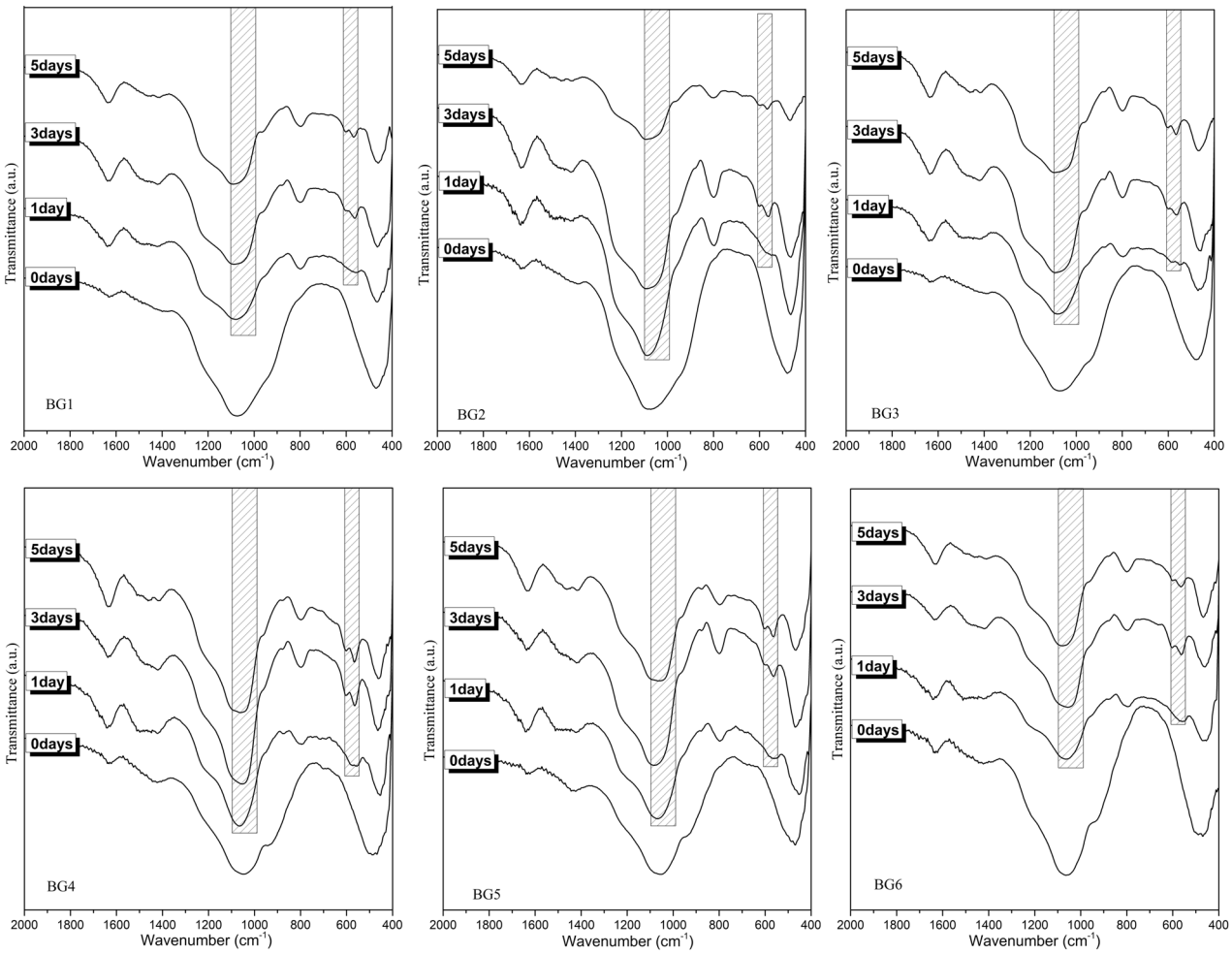

Fig. 7 FTIR spectra of all samples after 0, 1, 3, and 5 days of immersion in SBF

amorphous phase on the surface of the samples after 24 h and the formation of apatite after 3 days of immersion. Moreover, after 5 days of immersion, the double peak around 550–610 cm^{-1}, along with the further sharpening of the broad peak around 900–1200 cm^{-1} revealed further crystallization of an HAp phase.

After 24 h of immersion, SEM microphotographs (Fig. 8) and EDS analysis revealed the formation of an amorphous Ca-P phase on the surface of the grains of BG1, BG2, BG4, BG5, and BG6, with a mean molar Ca/P ratio quite below 1.67, which is common to non-stoichiometric apatites [66]. SEM microphotographs of **BG3** revealed the appearance of small agglomerated apatite spheres due to the Hap layer formation on the surface of the grains, with mean Ca/P molar ratio around 1.67 after 24 h. EDS analysis revealed a mean molar ratio of Ca/P around to 1,67 after 5 days of immersion for all samples.

XRD patterns of all bioactive glasses before and after 24 h and 3 days of immersion in SBF are shown in Fig. 9. According to XRD analysis, the percentages of the identified crystalline phases confirmed a gradual crystallization of a hydroxyapatite phase by the progressive formation of the peaks attributed to hydroxyapatite. More specifically, after 24 h of immersion the high amount of amorphous phase of all bioactive glasses was decreased, while amounts of HAp (5–7%) and Calcium Phosphate (3–10%) were identified. Moreover, the XRD patterns of samples BG4, BG5 and BG6 indicate that calcite, the more stable polymorph of the three predominant anhydrous calcium carbonate mineral phases of $CaCO_3$, with the other two being aragonite and vaterite, has been formed. After 3 days of immersion, the percentage of the crystalline phase of HAp was further increased (up to 21% for samples BG1, BG2 and BG3).

3.7 Hemolytic properties of representative BG3

The hemolytic activity of BG3 was evaluated, based on its optimum bioactive behavior. The hemolysis assay is commonly performed at body and fever temperature (37 °C,

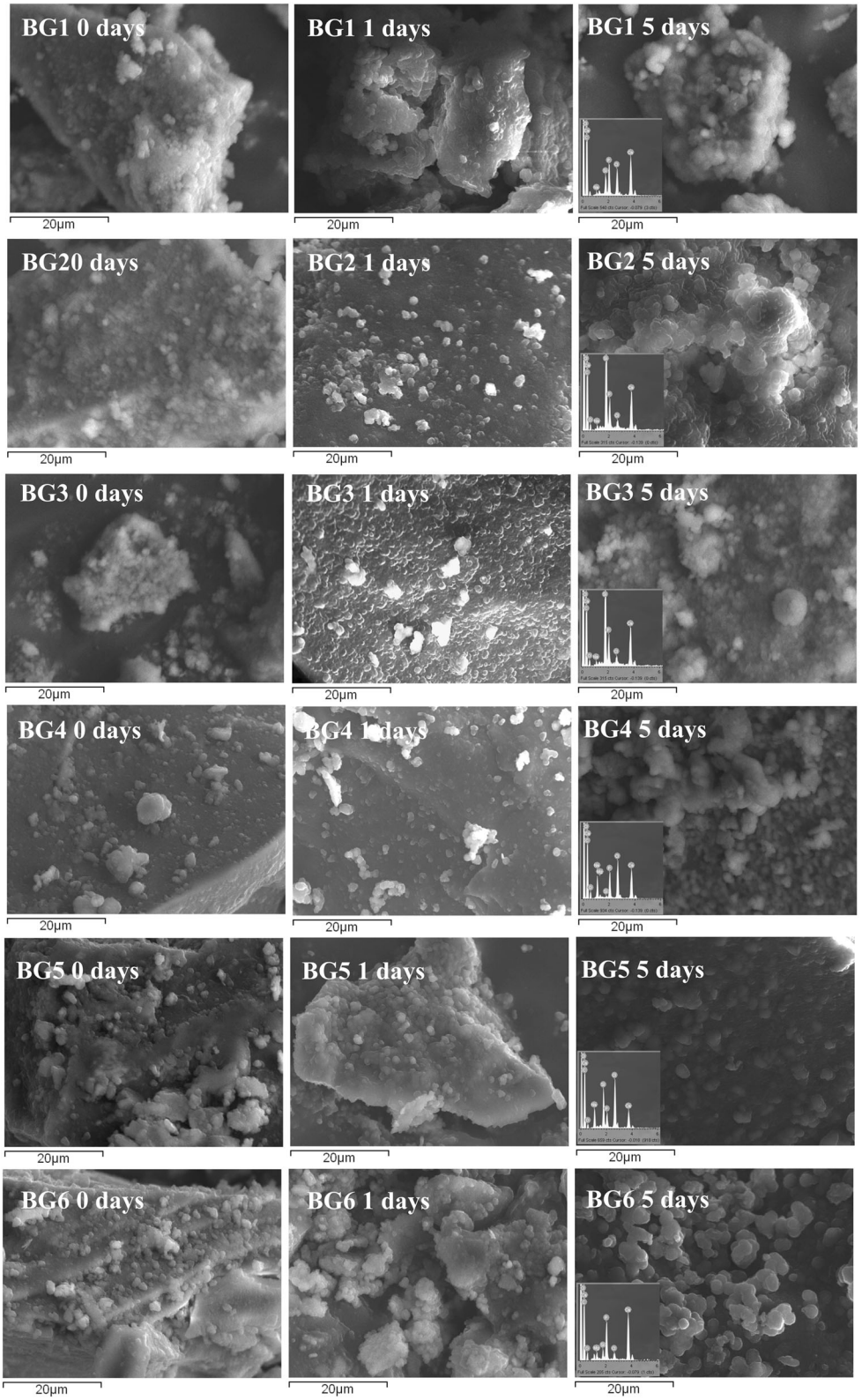

Fig. 8 SEM microphotographs of all samples before the immersion in SBF and after 1day and 5 days of immersion respectively

41 °C) at concentrations ranging from 0.25 to 7.5 mg/ml till 48 h of incubation. BG3 induced dose-dependent hemolysis on Red blood cell (RBC) after the first 24 h of incubation. Furthermore its hemolytic activity increased with fever temperature in line with previous findings of other tested nanoparticles [67]. It didn't reveal any hemolytic activity in

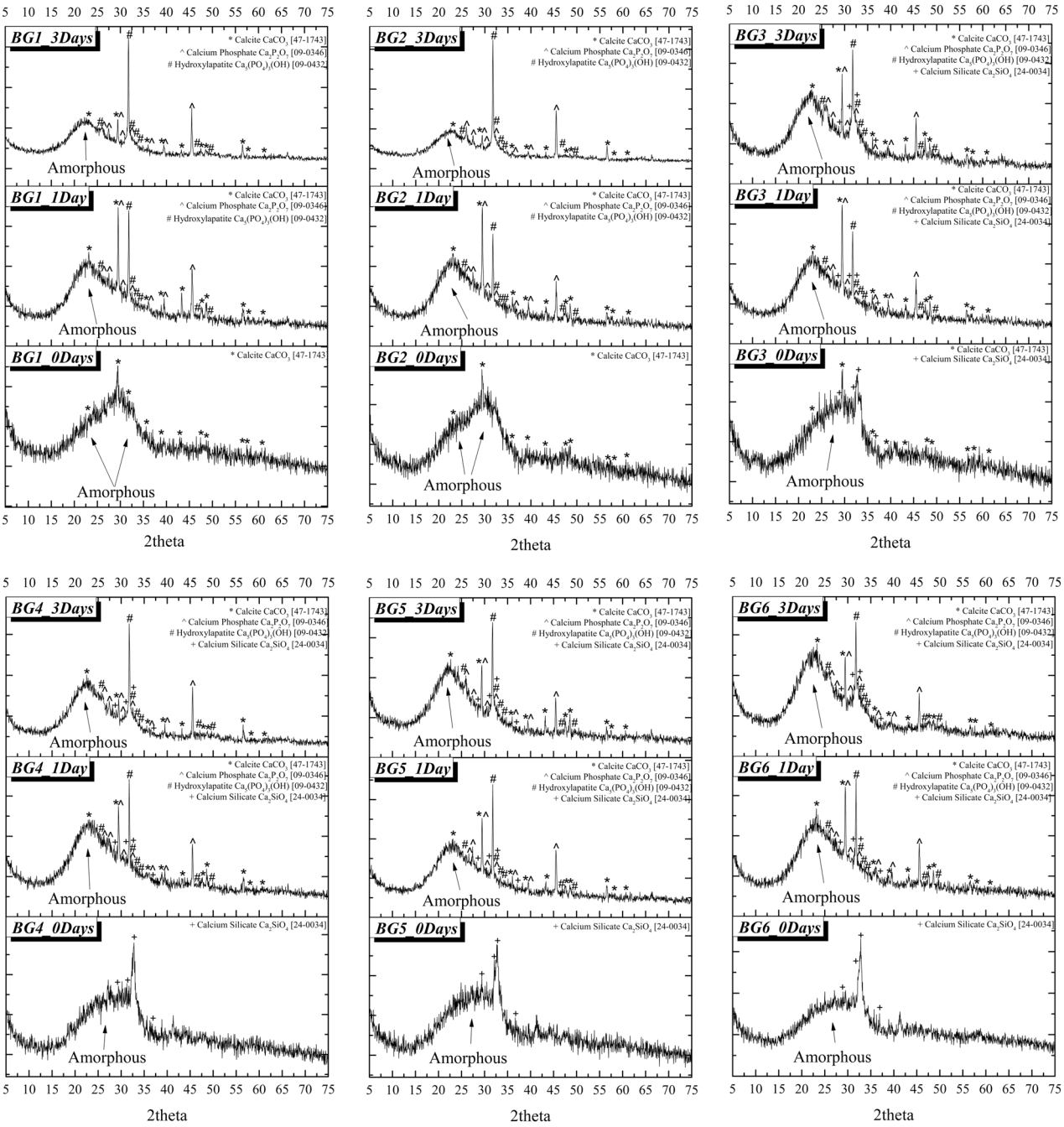

Fig. 9 XRD patterns of all samples before (0 days) and after 24 h and 3 days of immersion in SBF

dosages under 1 mg/ml at body temperature. When measured at fever temperature (41 °C) a twofold increase in hemolysis at low dosages (0.25 and 0.5 mg/ml) was observed. Based on the large hemolysis dependence on fever temperature, all dosages below 0.25 mg/ml can be considered as non-hemolytic concentrations (Fig. 10a). It is noteworthy that after 24 h of incubation there wasn't any further increase of the haemolytic activity. Moreover, there wasn't any coagulation of the RBCs upon treatment, and no interferences in the absorptions from 500 to 700 nm occurred with the selected BG nanomaterial (Fig. 10b). According to ASTMF756–00(2000) standard, the hemolytic value above 2% was considered as hemolytic and the value less than 2% was considered as non hemolytic. This indicates that BG3 possesses good hemocompatibility, which is essential for its applications in bone tissue engineering.

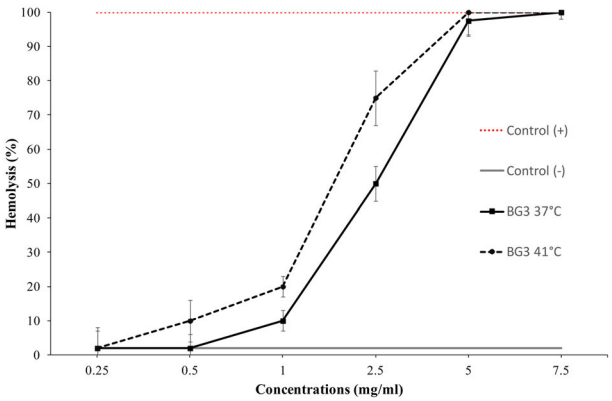

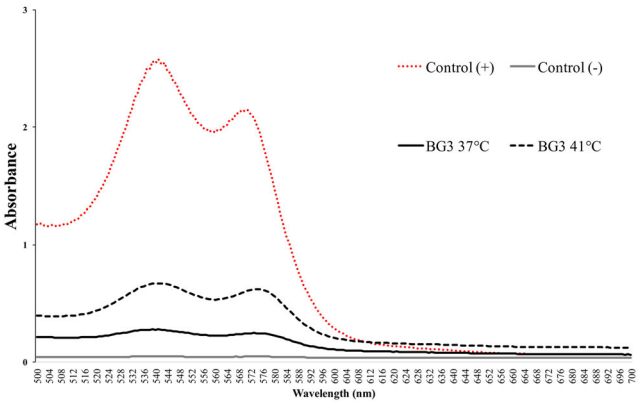

Fig. 10 Hemolysis assay on selected bioactive glass nanoparticle (BG3). **a** Hemolysis activity of human RBCs upon incubation with selected bioactive glass nanoparticle (BG3) at different concentrations (0.25, 0.5, 1, 2.5, 5, 7.5 mg/ml) and different temperatures (37, 41 °C) after 24 h of incubation. **b** Absorbance values (500–700) of the hemolysis assay of Controls (+, –) and the presence of the bioactive glass nanoparticle (BG3) at a concentration of 1 mg/ml. The presence of hemoglobin in the supernatant (red) was observed by spectrophotometry. The absorbance value of hemoglobin at 541 nm was measured with the reference wavelength of 700 nm. Data are the average ± SD of 5 independent experiments. * Significant differences to control (–) at $p < .05$ $**p < .001$ The percent of hemolysis was calculated as follows: Hemolysis % = [(sample absorbance - negative control)/(positive control - negative control)] * 100%

Table 2 Effect of BG3 (0.5 mg/ml) on the growth parameters of seven bacterial strains. Data were normalized and combined from three separate runs with triplicate samples ($n = 9$)

Challenge organism	Maximum growth rate (h^{-1})		Lag phase (h)	
	Ratio BG3: control	T-Test P value	Control	BG3
Listeria monocytogenes	1.22	0.1272	1.7	1.5
Bacillus cereus	0.79[a]	0.0034	1.0	0.9
Staphylococcus aureus	0.87[a]	<0.0001	1.0	1.0
Escherichia coli	1.11	0.0953	0.5	0.5
Salmonella Typhimurium	1.04	0.6774	0.8	0.7
Salmonella Enteritidis	1.11	0.3423	0.9	0.8
Pseudomonas aeruginosa	0.83[a]	0.0293	2.3	2.1

[a]Significant reduction in growth rate

3.8 Antibacterial properties of BG3

The results of the microbiological challenge testing of BG3 are given in Table 2 below. A small but significant ($P < 0.05$) decrease in growth rate in the presence of BG3 was observed for *Bacillus cereus, Staphylococcus aureus*, and *Pseudomonas aeruginosa*, but the growth rates of *Listeria monocytogenes, Escherichia coli* and two serotypes of *Salmonella enterica* were not affected. Estimated lag phases of all tested strains were unaffected by BG3.

4 Discussion

Calcium magnesium silicates are regarded as bioactive ceramics for bone tissue regeneration due to their enhanced osteoconductivity and improved bioactivity. Mg-containing bioceramics with enhanced apatite forming ability, osteoconductivity and mechanical properties have previously been fabricated, including glass-ceramics in the system SiO_2–CaO–MgO, akermanite and bredigite [50, 52]. Despite, the osteoinductive behavior and connectivity ability of such ceramics, angiogenesis is still a problem. As copper presents angiogenic properties, its incorporation in various bioceramic materials could enhance their angiogenic profile. At the same time, the introduction of copper into the glass composition can be beneficial, due to the antimicrobial/antibacterial properties of copper. Hemocompatibility on the other hand, has been considered as one of the key issues for an ideal material to be used in bond tissue engineering applications, especially when the designed materials are required to contact blood. Taking all the above into account, the need for hemocompatible materials that combine apatite forming ability with antibacterial properties are promising for bone tissue engineering applications. For these reasons, in this work, the synthesis of six different Cu-containing calcium magnesium silicate materials was performed through the sol–gel method. Although sol-gel is a well-established synthesis method, various parameters can improve or restrict the properties of the final product. Thus optimum synthesis conditions are necessary for an augmented outcome.

In the present study, the synthesized samples were categorized in two groups according to the amount of the added ammonia; the first group (BG1–BG3) included the samples produced by the addition of the highest amount of ammonia and the second group (BG4–BG6), those with the lowest amount. The results showed that all samples were capable of hydroxyapatite formation. However, according to FTIR, SEM-EDS and XRD results after soaking in SBF

for 24 h, apatite formation starts earlier on the sample BG3 compared to the other samples, whose spectra revealed the formation of an amorphous phase and the formation of apatite only after 3 days of immersion. As apatite formation is strongly dependent on the particle size, higher bioactivity should impose smaller particle size for the BG3. This can be justified by the high specific surface area observed in particles of small size that enhances BGs contact surface area with SBF, which increases their biodegradation [68]. On the other hand, the concentration of ammonia is one of the main parameters, which governs the particle size of the sol–gel synthesized nanomaterials [23] but the final size results from very complex reactions and dependents on many factors acting simultaneously, such as the water and ammonia concentration, type of alkoxides and alcohol used [69, 70]. SEM microphotographs in the present study revealed highly dispersed smaller particles for Group A materials and especially for BG3, which is in agreement to the findings of many studies regarding the role of ammonia in increasing the dispersion rate of nanoparticles [71], but contradict other studies that have shown increased particle size with increased ammonia concentration [72, 73]. This can be explained as follows: BG3 differed compared to BG1 and BG2 in that it was synthesized with the lowest H_2O/ethanol ratio, meaning that high amounts of ethanol were introduced. It has been reported that low quantity of water and high amount of ethanol results in smaller particle size, due to the reduction of the hydrolysis rate through bonding between ethanol and water molecules [74]. Small and well dispersed particles increase surface area and thus provide more nucleation sites for apatite development, explaining in part the enhanced bioactivity of BG3 [68, 75]. Moreover, Group A consisted of materials with a small amount of the crystalline phase of calcite. At the early stages of immersion in SBF, calcium ions probably released from calcite, may have reacted with phosphates to speed up hydroxyapatite precipitation. Calcite is metastable under experimental conditions and in physiological conditions, and is expected to transform eventually to HAp [63]. So the presence of calcite which is a crystal phase known for its ability to bond to living bone [62], along with the simultaneous presence of the bioactive phase of Ca_2SiO_4 may have attributed to the enhanced bioactivity of BG3.

Despite the need of prevention against bacterial infection in orthopedic surgery due to the significant medical complications to patients related to infections, there are only a few antibiotic-free studies of calcium silicate bioactive glasses. Several research works have been mainly focused on the incorporation of antibacterial metallic ions, such as copper (Cu^{2+}), in bioactive glasses for bone regeneration applications. The incorporation of Cu^{2+} is mainly carried out because of its beneficial antibacterial behavior, which supports arresting and killing the growth of microbes at the implant site. In the present study the results of the microbiological testing revealed a small but significant ($P < 0.05$) decrease in growth rate in the presence of BG3 for *Bacillus cereus, Staphylococcus aureus*, and *Pseudomonas aeruginosa*. Various studies have reported that calcium silicate ceramics provide an antibacterial effect on Pseudomonas aeruginosa and Staphylococcus aureus. According to a previous study, Cu doped calcium silicate ceramics presented bactericidal effect on Staphylococcus aureus cultures and they can be considered as a suitable candidate to prevent infections and to treat bone defects [57, 76].

Previous studies have reported that nano-HA powders and porous HA-Mg materials have good blood compatibility, so they could be used for hard tissue regeneration applications. In the present study, the hemolytic effects of BG3 on human erythrocytes was tested, providing new insights for safety evaluation of new modified silica based nanoparticles. BG3 rupture erythrocytes in concentrations higher than 0,25 mg/ml, in contrast with other studies [72], where amorphous silica nanoparticles cause hemolysis even in very low concentrations such as 0.02 mg/ml. This difference could be attributed to variations of amorphous and crystalline structure which has been correlated to hemolytic behavior [58].

In future studies, the possible cytomembrane damage and/or the consequent oxidative damage of erythrocytes after exposure to different silica nanoparticles should be further investigated, in order to better improve their structure and consequently avoid the membrane injury.

5 Conclusion

In this study, six different bioactive nanomaterials were successfully synthesized through the sol–gel method, applying different ratios of ethanol/TEOS and ammonia amount. The optimum conditions were observed in the glass prepared with the highest ethanol/TEOS ratio and the highest amount of ammonia (BG3). Due to its enhanced apatite-forming ability and its antibacterial properties, this sol-gel synthesized nano-material, can be suggested in various tissue engineering processes.

Acknowledgements The authors wish to thank the PhD Candidate L. Malletzidou for performing the XRD measurements and Dr T. Zorba for assistance on FTIR measurements.

Compliance with ethical standards

Conflict of interest The authors declare that they have no conflict of interest.

References

1. Lavallee DK, Sullivan JC, Deutsch E. Reaction of thiols with the one-equivalent oxidants neptunium(VI) and cerium(IV) in aqueous acidic media. Inorg Chem 1973;12:1440–2.
2. Luz GM, Mano JF. Preparation and characterization of bioactive glass nanoparticles prepared by sol-gel for biomedical applications. Nanotechnology 2011;22:494014.
3. Ghalia MA, Dahman Y. Advanced nanobiomaterials in tissue engineering: synthesis, properties, and applications. In: Grumezescu AM, editor. Nanobiomaterials in Soft Tissue Engineering. Applications of Nanobiomaterials Volume 5. Oxford: William Andrew; 2016. pp.141–172.
4. Ghorbanian L, Emadi R, Razavi M, Shin H, Teimouri A. Synthesis and characterization of novel nanodiopside bioceramic powder. JNS. 2012;3:357–61.
5. Zhang W, Shen Y, Pan H, Lin K, Liu X, Darvell BW, et al. Effects of strontium in modified biomaterials. Acta Biomater Acta Mater Inc. 2011;7:800–8. https://doi.org/10.1016/j.actbio.2010.08.031.
6. Kankilic B, Köse S, Korkusuz P, Timuçin M, Korkusuz F. Mesenchymal stem cells and nano-bioceramics for bone regeneration. Curr Stem Cell Res Ther. 2016;11:487–93.
7. Vrancken KC, Possemiers K, Van Der Voort P, Vansant EF. Surface modification of silica gels with aminoorganosilanes. Colloids Surf A Physicochem Eng Asp. 1995;98:235–41.
8. Composites HO, Series ACSS, Society AC. Hybrid organic-inorganic composites; 1995.
9. Cerveau G, Corriu RJP, Lepeytre C, Mutin PH. Influence of the nature of the organic precursor on the textural and chemical properties of silsesquioxane materials. J Mater Chem. 1998;8:2707–13.
10. Corriu R. A new trend in metal-alkoxide chemistry: the elaboration of monophasic organic-inorganic hybrid materials. Polyhedron. 1998;17:925–34.
11. Corriu RJP, Leclercq D. Recent developments of molecular chemistry for sol–gel processes. Angew Chem Int Ed Engl. 1996;35:1420–36. https://doi.org/10.1002/anie.199614201f.
12. Shea KJ, Loy DA, Webster O. Arylsilsesquioxane gels and related materials. New hybrids of organic and inorganic networks. J Am Chem Soc. 1992;114:6700–10.
13. Jackson CL, Bauer BJ, Nakatani AI, Barnes JD. Synthesis of hybrid organic−inorganic materials from interpenetrating polymer network chemistry. Chem Mater 1996;8:727–33.
14. Nassar EJ, Ciuffi KJ, Ribeiro SJL, Messaddeq Y. Europium incorporated in silica matrix obtained by sol-gel: luminescent materials. Mater Res 2003;6:557–62.
15. Beari F, Brand M, Jenkner P, Lehnert R, Metternich HJ, Monkiewicz J, et al. Organofunctional alkoxysilanes in dilute aqueous solution: new accounts on the dynamic structural mutability. J Organomet Chem. 2001;625:208–16.
16. Nassar EJ, Neri CR, Calefi PS, Serra OA. Functionalized silica synthesized by sol-gel process. J Non Cryst Solids. 1999;247:124–8.
17. Stober W, Fink A, Bohn E. Controlled growth of monodisperse silica spheres in the micron size range. J Colloid Interface Sci. 1968;26:62–9.
18. Papacídero AT, Rocha LA, Caetano BL, Molina E, Sacco HC, Nassar EJ, et al. Preparation and characterization of spherical silica-porphyrin catalysts obtained by the sol-gel methodology. Colloids Surf A Physicochem Eng Asp. 2006;275:27–35.
19. Nassar EJ, Nassor ECDO, Ávila LR, Pereira PFS, Cestari A, Luz LM, et al. Spherical hybrid silica particles modified by methacrylate groups. J Sol Gel Sci Technol. 2007;43:21–6.
20. Ricci GP, Rocha ZN, Nakagaki S, Castro KADF, Crotti AEM, Calefi PS, et al. Iron-alumina materials prepared by the non-hydrolytic sol-gel route: Synthesis, characterization and application in hydrocarbons oxidation using hydrogen peroxide as oxidant. Appl Catal A Gen. 2010;389:147–54. https://doi.org/10.1016/j.apcata.2010.09.011.
21. Matos MG, Pereira PFS, Calefi PS, Ciuffi KJ, Nassar EJ. Preparation of a $GdCaAl_3O_7$ matrix by the non-hydrolytic sol-gel route. J Lumin 2009;129:1120–4.
22. Castillo-León J, Andersen K, Svendsen W. Self–Assembled Peptide Nanostructures for Biomedical Applications: Advantages and Challenges. In: Pignatello R, editor. Biomterials Science and Engineering. Rijeka, InTech; 2011. pp.115–38.
23. Jafarzadeh M, Rahman IA, Sipaut CS. Synthesis of silica nanoparticles by modified sol-gel process: The effect of mixing modes of the reactants and drying techniques. J Sol Gel Sci Technol. 2009;50:328–36.
24. Hench LL, West JK. CH2-23-28 (sol-gel and base catalyst explain). Chem Rev 1990;90:33–72.
25. Chu L, Tejedor-Tejedor MI, Anderson MA. Particulate sol-gel route for microporous silica gels. Microporous Mater 1997;8:207–13.
26. Meixner DL, Dyer PN. Influence of sol-gel synthesis parameters on the microstructure of particulate silica xerogels. J Sol Gel Sci Technol. 1999;14:223–32.
27. Colomer MT, Anderson MA. High porosity silica xerogels prepared by a particulate sol-gel route: pore structure and proton conductivity. J Non Cryst Solids. 2001;290:93–104.
28. Enomoto N, Kumagai A, Hojo J. Aging effect of starting solutions for spherical silica synthesis. J Ceram Soc Japan. 2005;113:340–3.
29. Bogush GH, Zukoski CF. Uniform silica particle precipitation: an aggregative growth model. Chem Eng 1991;142:19–34.
30. Van Helden AK, Jansen JW, Vrij A. Preparation and characterization of spherical monodisperse silica dispersions in nonaqueous solvents. J Colloid Interface Sci. 1981;81:354–68.
31. Tan C, Bowen B, Epstein N. Production of monodisperse colloidal silica spheres: effect of temperature. J Colloid Interface Sci. 1987;118:290–3.
32. Enomoto N, Koyano T, Nakagawa ZE. Effect of ultrasound on synthesis of spherical silica. Ultrason Sonochem 1996;3:3–7.
33. Chen S, Dong P. The size dependence of growth rate of monodisperse silica particles from tetraalkoxysilane. J Colloid Interface Sci. 1997;272:268–72.
34. Sadasivan S, Rasmussen DH, Chen FP, Kannabiran RK. Preparation and characterization of ultrafine silica. Colloids Surf A Physicochem Eng Asp. 1998;132:45–52.
35. Lee K, Sathyagal AN, McCormick AV. A closer look at an aggregation model of the Stöber process. Colloids Surf A Physicochem Eng Asp. 1998;144:115–25.
36. Park SK, Kim KDo, Kim HT. Preparation of silica nanoparticles: determination of the optimal synthesis conditions for small and uniform particles. Colloids. Surf A Physicochem Eng Asp. 2002;197:7–17.
37. Green DL, Jayasundara S, Lam YF, Harris MT. Chemical reaction kinetics leading to the first Stober silica nanoparticles—NMR and SAXS investigation. J Noncryst Solids. 2003;315:166–79.
38. Green DL, Lin JS, Lam YF, Hu MZC, Schaefer DW, Harris MT. Size, volume fraction, and nucleation of Stober silica nanoparticles. J Colloid Interface Sci. 2003;266:346–58.
39. Nagao D, Osuzu H, Yamada A, Mine E, Kobayashi Y, Konno M. Particle formation in the hydrolysis of tetraethyl orthosilicate in pH buffer solution. J Colloid Interface Sci. 2004;279:143–9.
40. No YJ, Roohaniesfahani S, Lu Z, Shi J, Zreiqat H. Strontium-doped calcium silicate bioceramic with enhanced in vitro osteogenic properties. Biomed Mater 2017;12:035003.
41. Lin K, Xia L, Li H, Jiang X, Pan H, Xu Y, et al. Biomaterials enhanced osteoporotic bone regeneration by strontium-substituted calcium silicate bioactive ceramics. Biomaterials. 2013;34:10028–42.

42. Xu S, Lin K, Wang Z, Chang J, Wang L, Lu J, et al. Reconstruction of calvarial defect of rabbits using porous calcium silicate bioactive ceramics. Biomaterials. 2008;29:2588–96.
43. Wang C, Lin K, Chang J, Sun J. Osteogenesis and angiogenesis induced by porous β-$CaSiO_3$/PDLGA composite scaffold via activation of AMPK/ERK1/2 and PI3K/Akt pathways. Biomaterials. 2013;34:64–77. https://doi.org/10.1016/j.biomaterials.2012.09.021.
44. Wang C, Xue Y, Lin K, Lu J, Chang J, Sun J. The enhancement of bone regeneration by a combination of osteoconductivity and osteostimulation using β-$CaSiO_3$/β-$Ca_3(PO_4)_2$ composite bioceramics. Acta Biomater. 2012;8:350–60. https://doi.org/10.1016/j.actbio.2011.08.019.
45. Zhu Y, Zhu M, He X, Zhang J, Tao C. Substitutions of strontium in mesoporous calcium silicate and their physicochemical and biological properties. Acta Biomater. 2013;9:6723–31. https://doi.org/10.1016/j.actbio.2013.01.021.
46. Zreiqat H, Ramaswamy Y, Wu C, Paschalidis A, Lu ZF, James B, et al. The incorporation of strontium and zinc into a calcium-silicon ceramic for bone tissue engineering. Biomaterials. 2010;31:3175–84. https://doi.org/10.1016/j.biomaterials.2010.01.024.
47. Ni GX, Shu B, Huang G, Lu WW, Pan HB. The effect of strontium incorporation into hydroxyapatites on their physical and biological properties. J Biomed Mater Res. 2012;100 B:562–8.
48. Ramaswamy Y, Wu C, Zhou H, Zreiqat H. Biological response of human bone cells to zinc-modified Ca-Si-based ceramics. Acta Biomater. 2008;4:1487–97.
49. Chen X, Ou J, Wei Y, Huang Z, Kang Y, Yin G. Effect of MgO contents on the mechanical properties and biological performances of bioceramics in the MgO-CaO-SiO_2 system. J Mater Sci Mater Med. 2010;21:1463–71.
50. Wu C, Ramaswamy Y, Zreiqat H. Porous diopside ($CaMgSi_2O_6$) scaffold: a promising bioactive material for bone tissue engineering. Acta Biomater. 2010;6:2237–45.
51. Wu C, Ramaswamy Y, Soeparto A, Zreiqat H. Incorporation of titanium into calcium silicate improved their chemical stability and biological properties. J Biomed Mater Res. 2008;86:402–10.
52. Goudouri OM, Kontonasaki E, Chrissafis K, Zinn K, Hoppe A, Detsch R, et al. Towards the synthesis of an Mg-containing silicate glass-ceramic to be used as a scaffold for cementum/alveolar bone regeneration. Ceram Int. 2014;40:16287–98.
53. Diba M, Goudouri OM, Tapia F, Boccaccini AR. Magnesium-containing bioactive polycrystalline silicate-based ceramics and glass-ceramics for biomedical applications. Curr Opin Solid State Mater. 2014;18:147–67. https://doi.org/10.1016/j.cossms.2014.02.004.
54. Hoppe A, Meszaros R, Stähli C, Romeis S, Schmidt J, Peukert W, et al. In vitro reactivity of Cu doped 45S5 Bioglass® derived scaffolds for bone tissue engineering. J Mater Chem B 2013;1:5659.
55. Hoppe A, Güldal NS, Boccaccini AR. A review of the biological response to ionic dissolution products from bioactive glasses and glass-ceramics. Biomaterials. 2011;32:2757–74. https://doi.org/10.1016/j.biomaterials.2011.01.004.
56. Theodorou GS, Kontonasaki E, Theocharidou A, Bakopoulou A, Bousnaki M, Hadjichristou C, et al. Sol-gel derived Mg-based ceramic scaffolds doped with zinc or copper ions: preliminary results on their synthesis, characterization, and biocompatibility. Int J Biomater. 2016;2016:3858301.
57. Kaya S, Cresswell M, Boccaccini AR. Mesoporous silica-based bioactive glasses for antibiotic-free antibacterial applications. Mater Sci Eng C. 2018;83:99–107. https://doi.org/10.1016/j.msec.2017.11.003.
58. Skaug V, Gylseth B. Hemolytic activity of five different calcium silicates. Environ Health Perspect. 1983;51:195–203.
59. El-Kady AM, Farag MM. Bioactive glass nanoparticles as a new delivery system for sustained 5-fluorouracil release: characterization and evaluation of drug release mechanism. J Nanomater. 2015;2015:1–11.
60. Kokubo T, Kushitani H, Sakka S, Kitsugi T, Yamamum T. Surface-structure changes in bioactive. J Biomed Mater Res. 1990;24:721–34.
61. Zhang Y, Mizuno M, Yanagisawa M, Takadama H. Bioactive behaviors of porous apatite- and wollastonite-containing glass-ceramic in two kinds of simulated body fluid. J Mater Res. 2003;18:433–41.
62. Van Helden AK, Jansen JW, Vrij A. Preparation and Characterization of Spherical Monodisperse Silica Dispersions in Non-aqueous Solvents. J Colloid Interface Sci. 1981;81: 354–68.
63. Smith B. Infrared spectral interpretation: a system approach. CRC Press LLC; 2000.
64. Ogino M, Ohuchi F, Hench LL. Compositional dependence of the formation of calcium phosphate films on bioglass. J Biomed Mater Res. 1980;14:55–64.
65. Filgueiras MRT, La Torre G, Hench LL. Solution effects on the surface reactions of three bioactive glass compositions. J Biomed Mater Res. 1993;27:1485–93.
66. Zorba T, Kantiranis N, Papadopoulou L, Chrissafis K, Giannoulatou V, Zachariadis G, et al. Magnesium calcium silicate bioactive glass doped with copper ions; synthesis and in-vitro bioactivity characterization. J Noncryst Solids. 2018;500:98–109.
67. Shi J, Hedberg Y, Lundin M, Odnevall Wallinder I, Karlsson HL, Möller L. Hemolytic properties of synthetic nano- and porous silica particles: the effect of surface properties and the protection by the plasma corona. Acta Biomater 2012;8:3478–90.
68. Lei B, Chen X, Han X, Zhou J. Versatile fabrication of nanoscale sol-gel bioactive glass particles for efficient bone tissue regeneration. J Mater Chem. 2012;22:16906–13.
69. Kim KDo, Kim HT. Formation of silica nanoparticles by hydrolysis of TEOS using a mixed semi-batch/batch method. J Sol Gel Sci Technol. 2002;25:183–9.
70. Kim TG, An GS, Han JS, Hur JU, Park BG, Choi SC. Synthesis of size controlled spherical silica nanoparticles via sol-gel process within hydrophilic solvent. J Korean Ceram Soc. 2017;54:49–54.
71. Su M, Su H, Du B, Li X, Ren G, Wang S. Mesoporous silica with monodispersed pores synthesized from the controlled self-assembly of silica nanoparticles. Korean J Chem Eng. 2015;32:852–9.
72. Kankilic B, Bayramli E, Kilic E, Dağdeviren S, Korkusuz F. Vancomycin containing PLLA/β-TCP controls MRSA in vitro. Clin Orthop Relat Res. 2011;469:3222–8.
73. Zeng D, Zhang H, Wang B, Sang K, Yang J. Effect of ammonia concentration on silica spheres morphology and solution hydroxyl concentration in stober process. J Nanosci Nanotechnol. 2015;15:7407–11.
74. Lukowiak A, Lao J, Lacroix J, Nedelec JM. Bioactive glass nanoparticles obtained through sol-gel chemistry. Chem Commun 2013;49:6620–2.
75. Mukundan LM, Nirmal R, Vaikkath D, Nair PD. A new synthesis route to high surface area sol gel bioactive glass through alcohol washing: a preliminary study. Biomatter 2013;3:1–10.
76. Bari A, Bloise N, Fiorilli S, Novajra G, Vallet-Regí M, Bruni G, et al. Copper-containing mesoporous bioactive glass nanoparticles as multifunctional agent for bone regeneration. Acta Biomater 2017;55:493–504.